Electronic Supplementary Material (ESI) for Sustainable Energy & Fuels.

Supporting information

Octanuclear Cu(II) cluster-tungstosilicate composite as efficient electrocatalyst for oxygen evolution at near-neutral pH

Junqi Lin*, Xin Chen, Nini Wang, Shanshan Liu, Yanmei Chen, Zhengfang Tian, Zhijun Ruan*

Hubei Key Laboratory of Processing and Application of Catalytic Materials, College of Chemistry and Chemical Engineering, Huanggang Normal University, Huanggang, 438000 China

* To whom correspondence should be addressed.

E-mail addresses: linjunqi@hgnu.edu.cn, ruanzhijun@hgnu.edu.cn

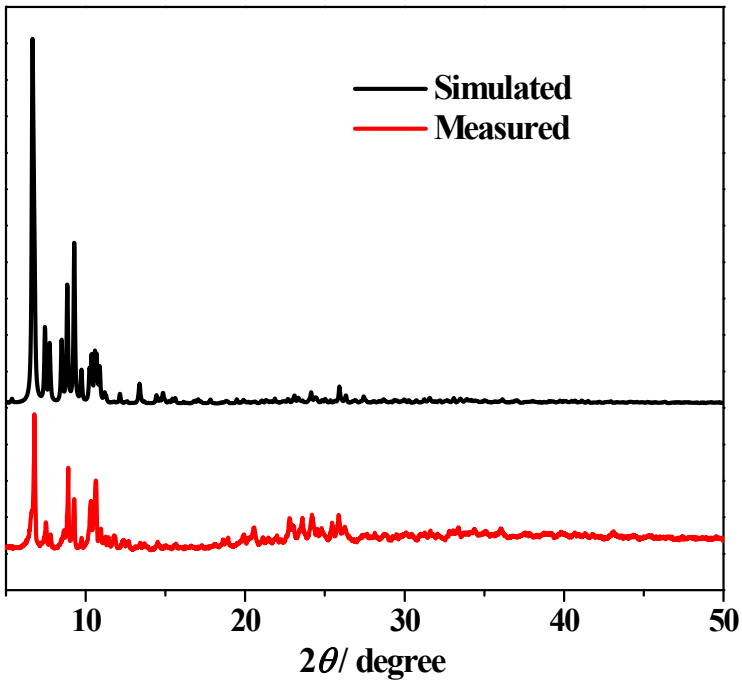

Fig. S1 Simulated powder X-ray diffraction data of $[Cu_8(dpk{\cdot}OH)_8(OAc)_4](ClO_4)_4{\cdot}9H_2O$ and measured PXRD data of synthesized Cu complex.

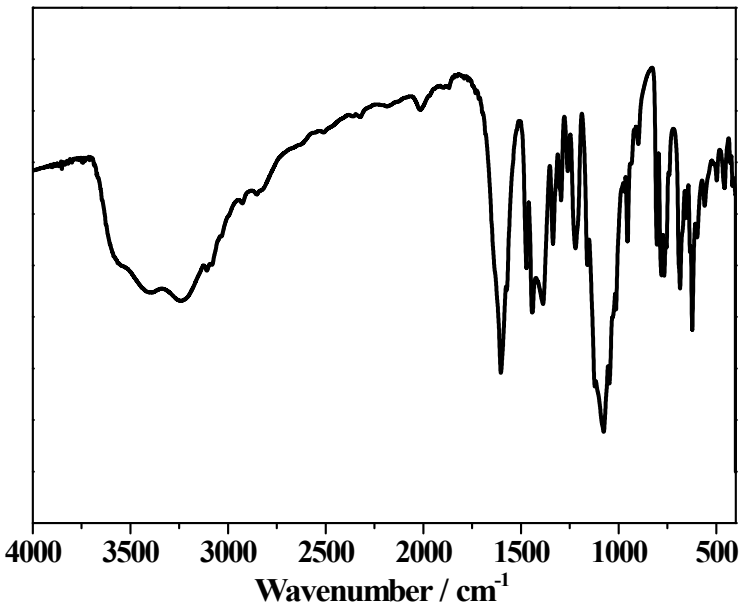

Fig. S2 FTIR spectrum of synthesized Cu complex: 1604 (s), 1472 (m), 1443 (s), 1221 (m), 1076 (vs), 956 (m), 805 (m), 779 (m), 767 (m), 684 (m), 623 (s).

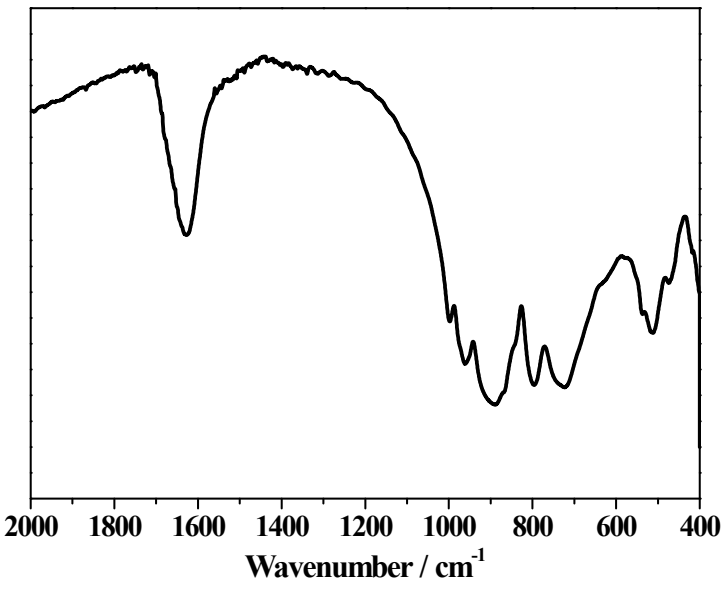

Fig. S3 FTIR spectrum of synthesized $K_8[\alpha\text{-}SiW_{11}O_{39}]$: 1000 (m), 952 (m), 885 (m), 870 (sh), 797 (m), 725 (m), 625 (m), 540 (m), 520 (m), 472(s), 430 (s).

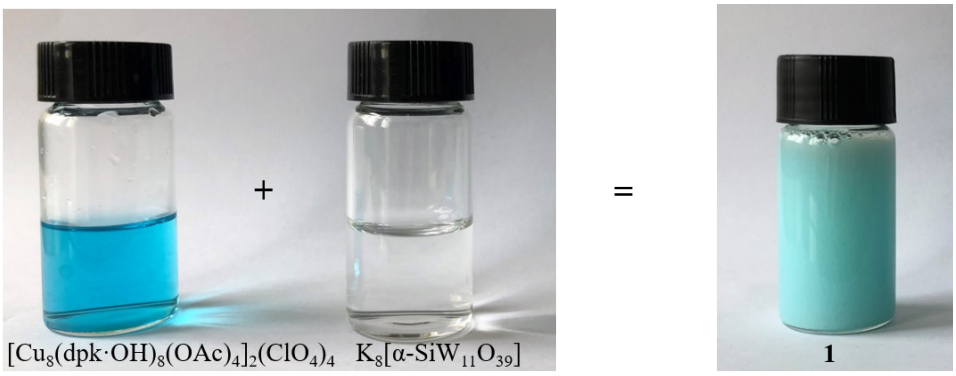

Fig. S4 Formation process of composite **1** $[Cu_8(dpk{\cdot}OH)_8(OAc)_4]_2$@$[\alpha\text{-}SiW_{11}O_{39}]$ in water.

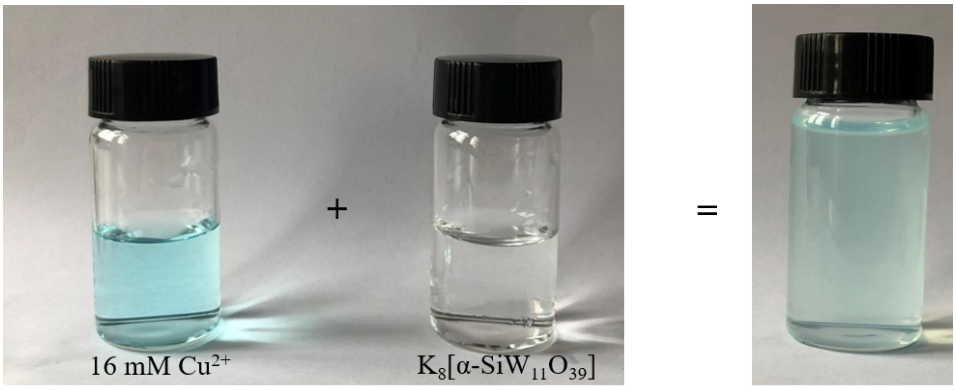

Fig. S5 Mixing of 16 mM Cu^{2+} and 0.2 mM $K_8[\alpha\text{-}SiW_{11}O_{39}]$ in water.

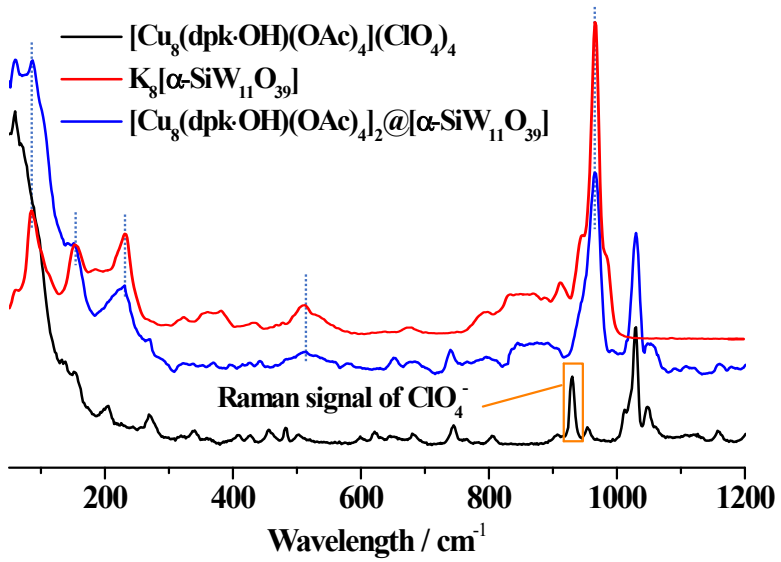

Fig. S6 Magnified Raman spectrum of composite **1**, $K_8[\alpha\text{-}SiW_{11}O_{39}]$ and Cu cluster.

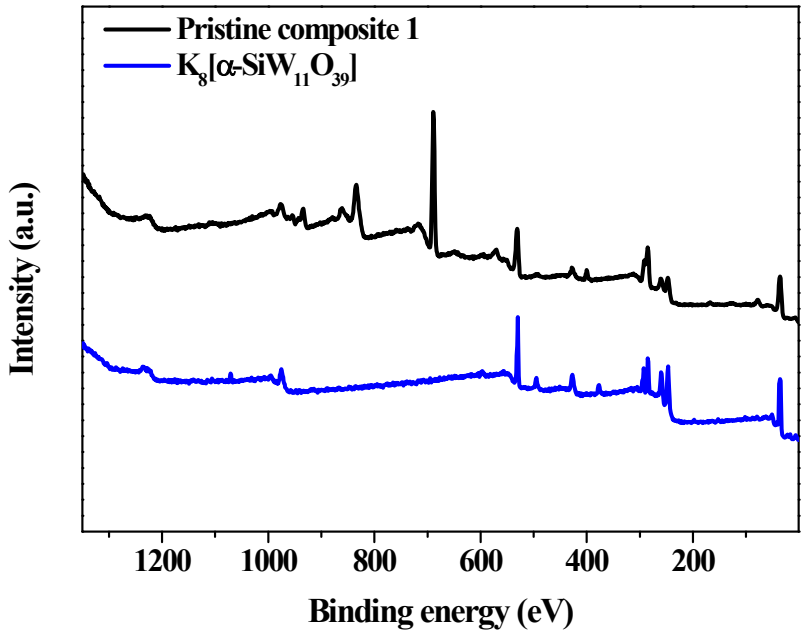

Fig. S7 XPS full scan spectra of composite **1** and polyoxometalate $K_8[\alpha\text{-}SiW_{11}O_{39}]$.

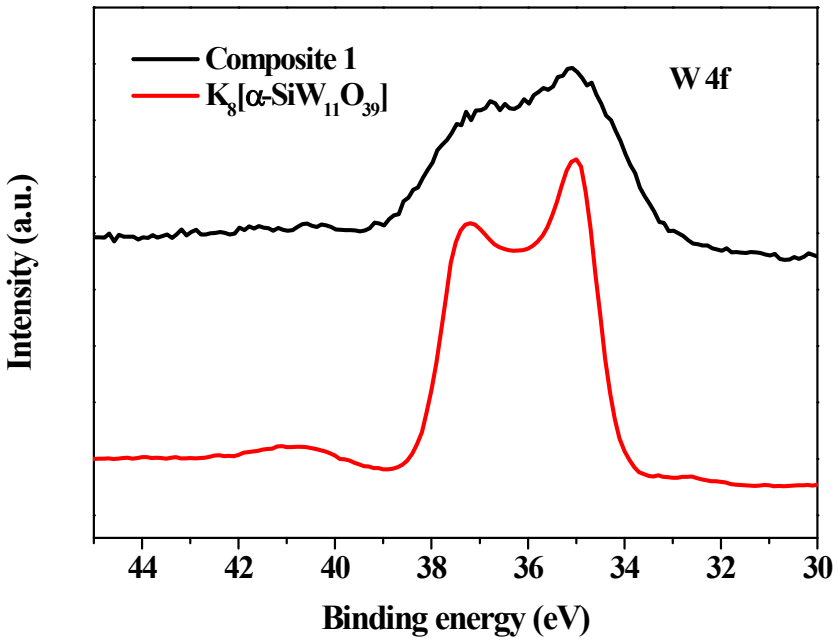

Fig. S8 High-resolution XPS W 4f spectra of composite **1** and polyoxometalate $K_8[\alpha\text{-}SiW_{11}O_{39}]$.

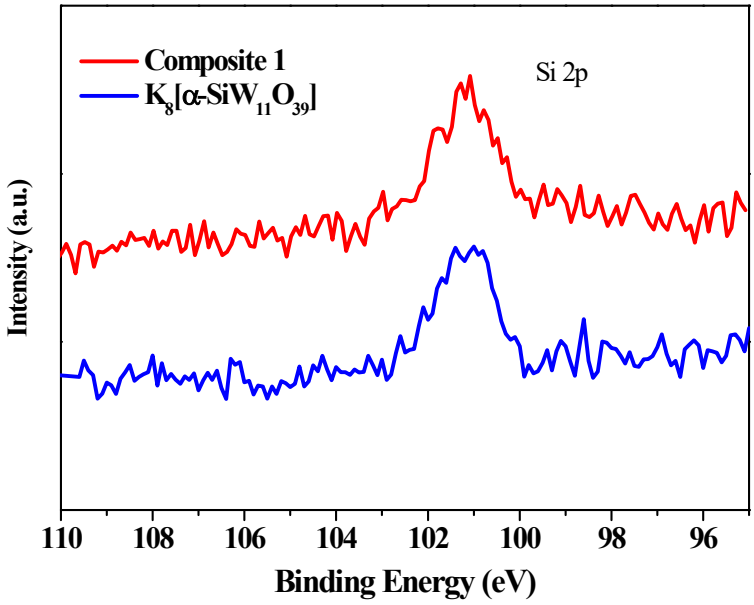

Fig. S9 High-resolution XPS Si 2p spectra of composite **1** and polyoxometalate $K_8[\alpha\text{-}SiW_{11}O_{39}]$.

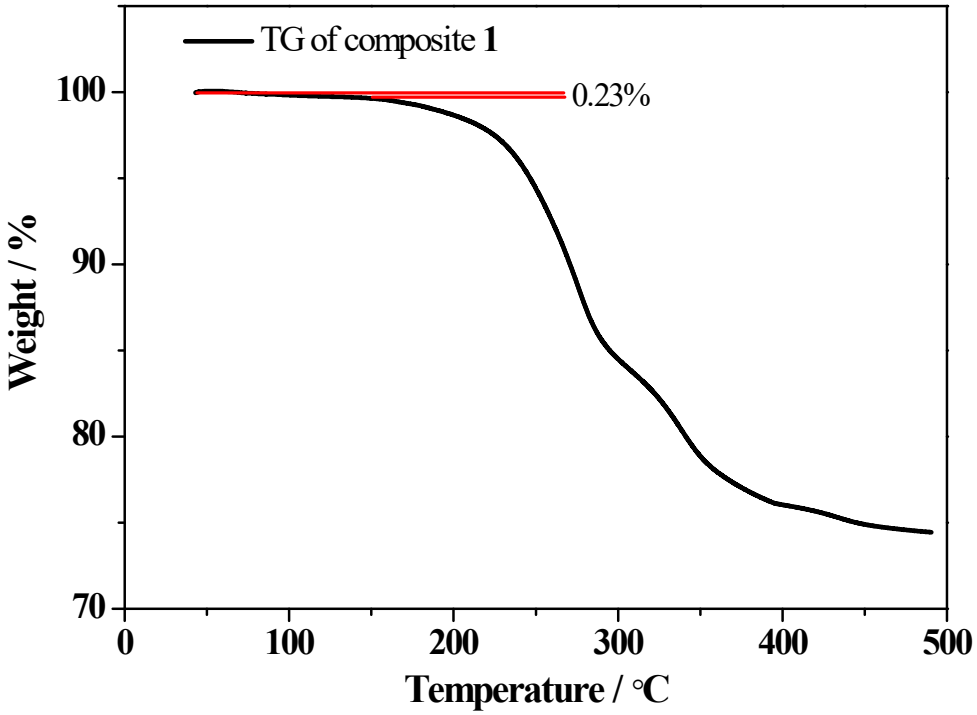

Fig. S10 TG analysis of composite **1** under N_2 atmosphere, temperature increasing rate: 10 °C / min.

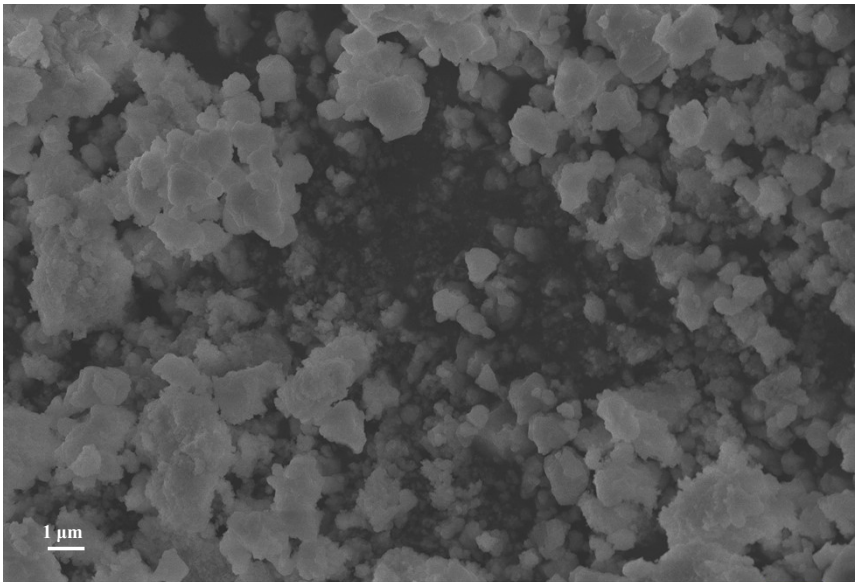

Fig. S11 The SEM images of the as-synthesized composite **1**.

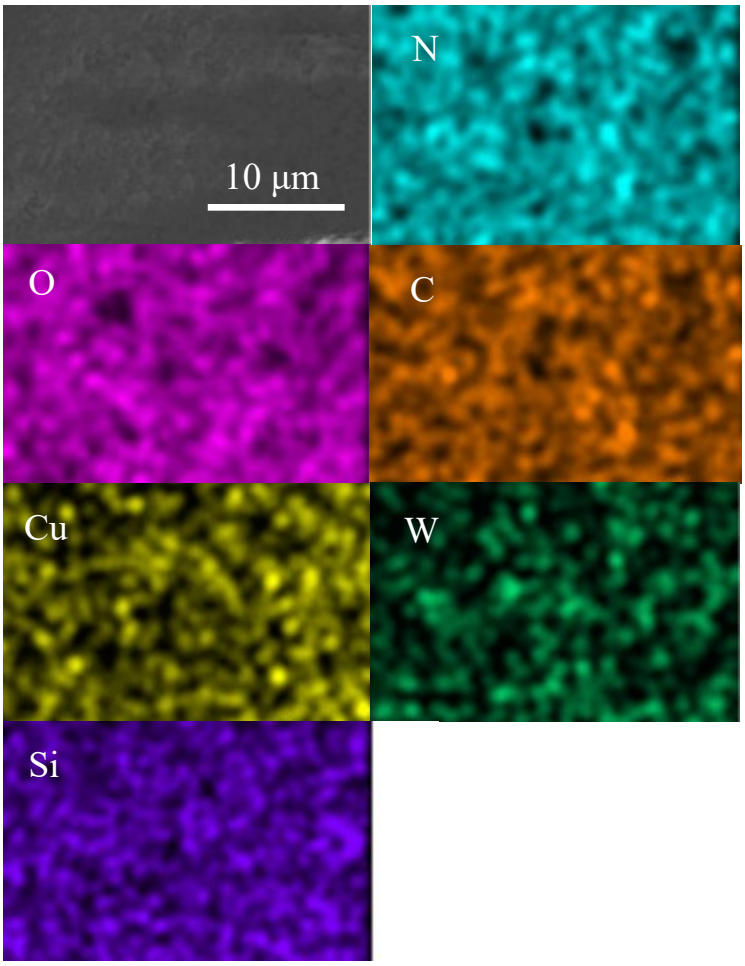

Fig. S12 EDS mapping images of the as-synthesized composite **1**.

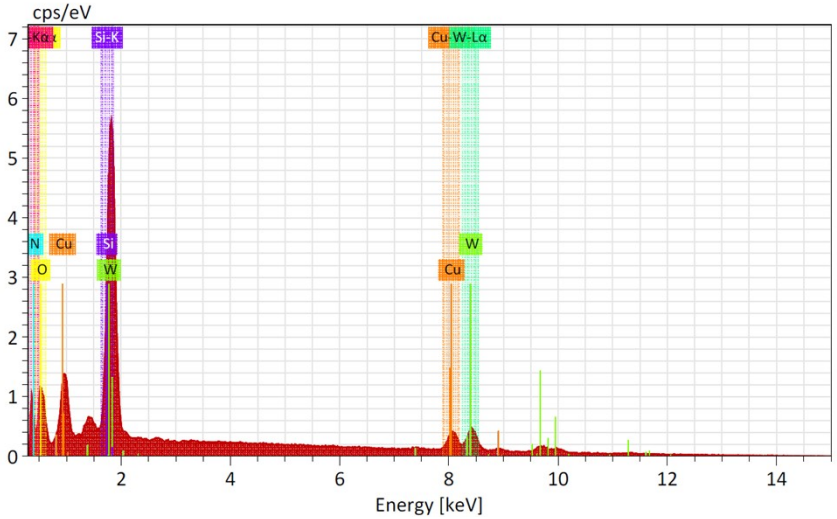

Fig. S13 EDS spectrum of the as-synthesized composite **1**.

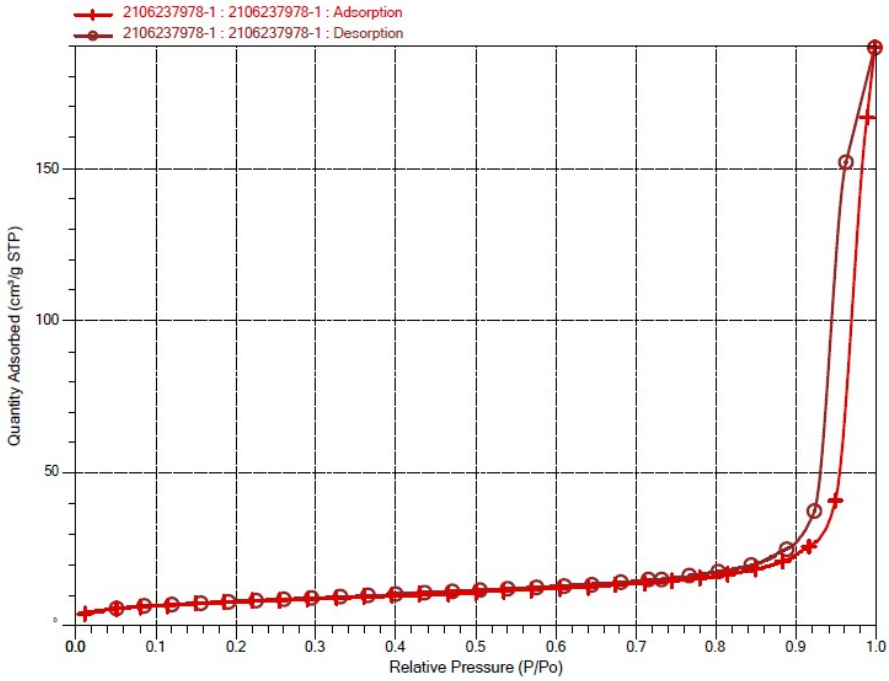

Fig. S14 The isotherm linear plot of the as-synthesized composite **1**.

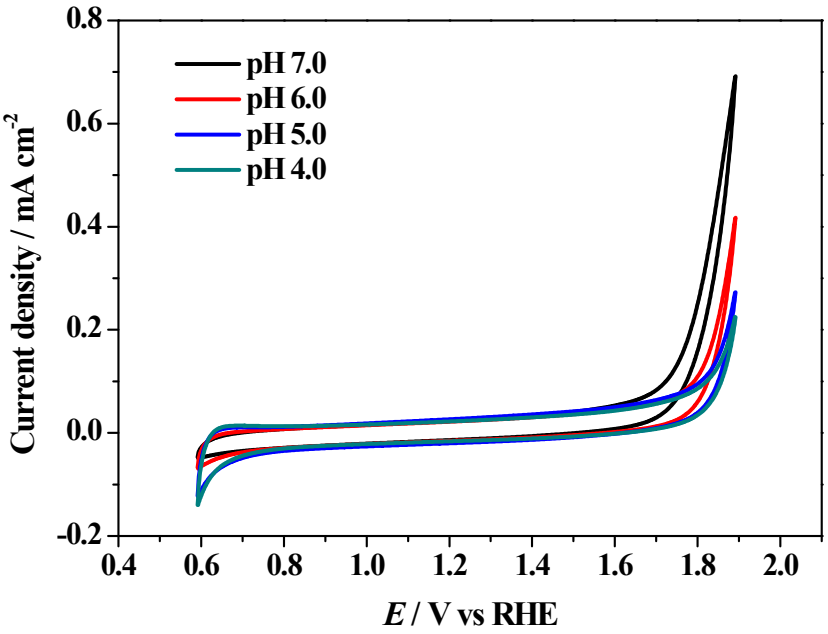

Fig. S15 CV test of 2 mM of $[Cu_8(dpk{\cdot}OH)_8(OAc)_4](ClO_4)_4$ in 0.1 M PBS at different pH, scan rate = 50 mV/s.

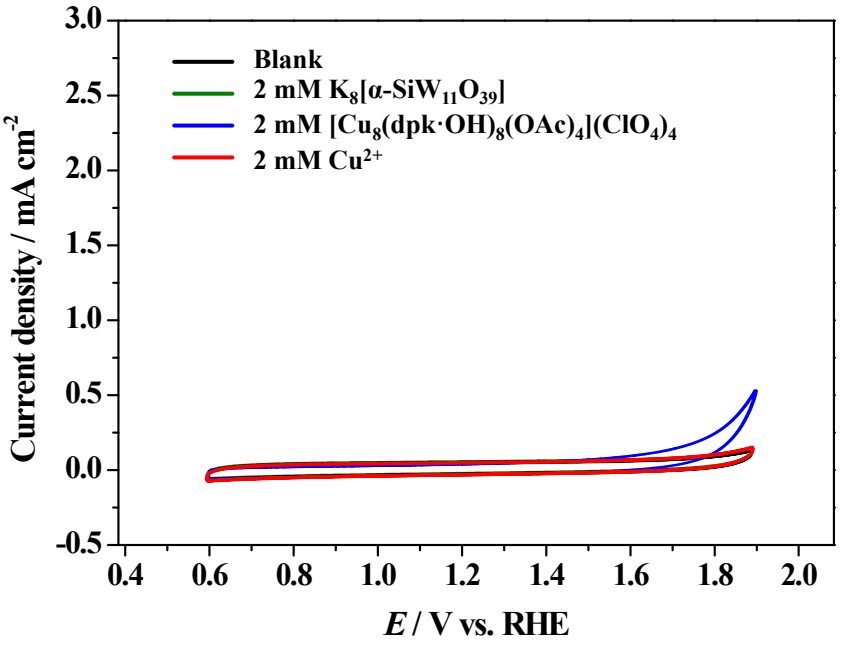

Fig. S16 CV curves of $[Cu_8(dpk{\cdot}OH)_8(OAc)_4](ClO_4)_4$, $K_8[\alpha\text{-}SiW_{11}O_{39}]$ and Cu^{2+} in PBS at pH of 6.5, scan rate=50 mV/s.

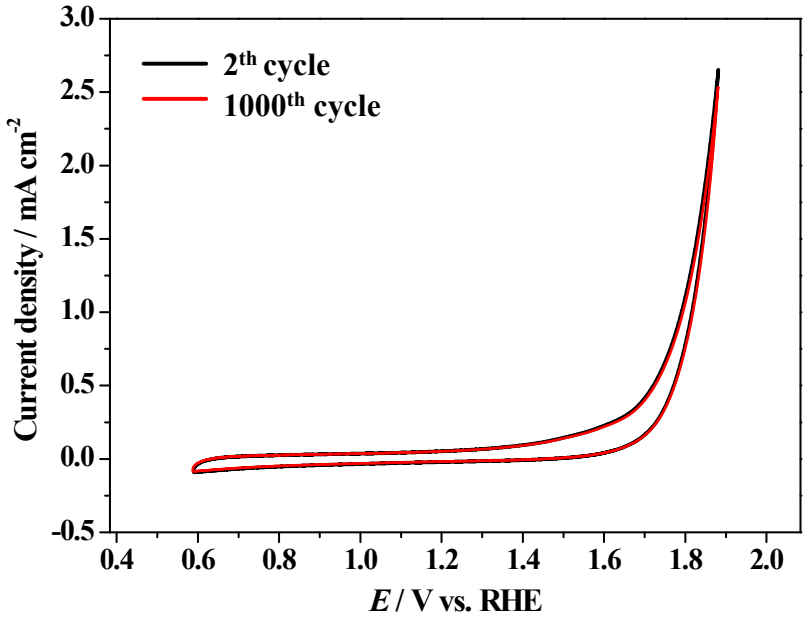

Fig. S17 Initial (2nd) CV curve and 1000th CV curve of composite **1** in PBS at pH=6.5, scan rate=50 mV/s.

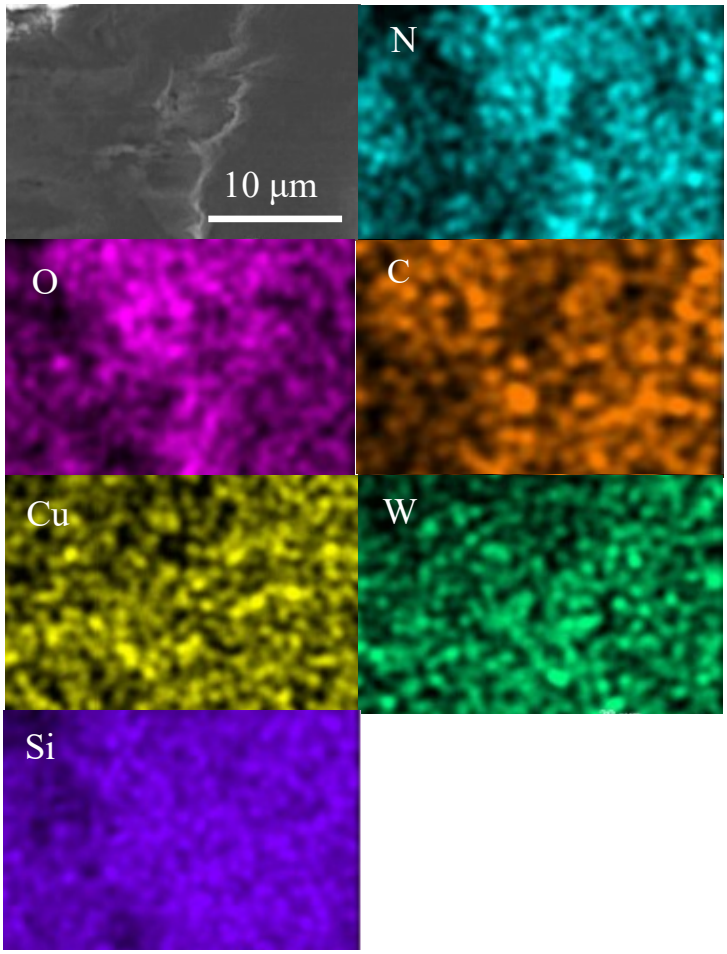

Fig. S18 EDS mapping images of the post-catalytic composite **1**.

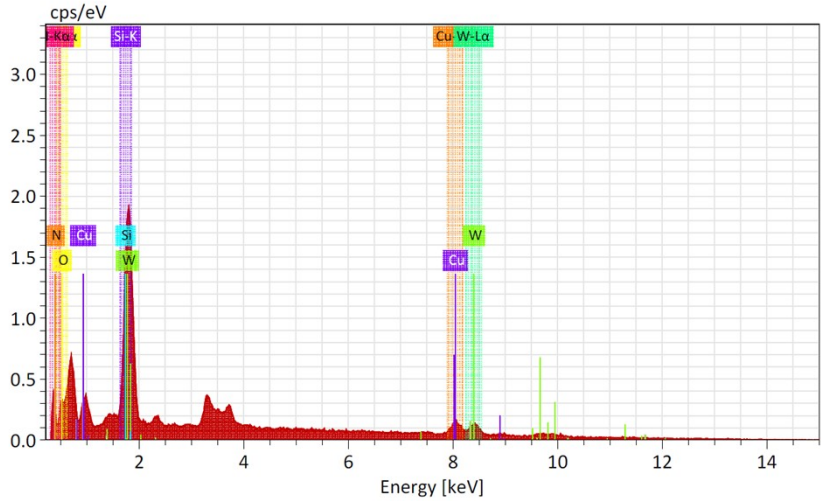

Fig. S19 EDS spectrum of the post-catalytic composite **1**.

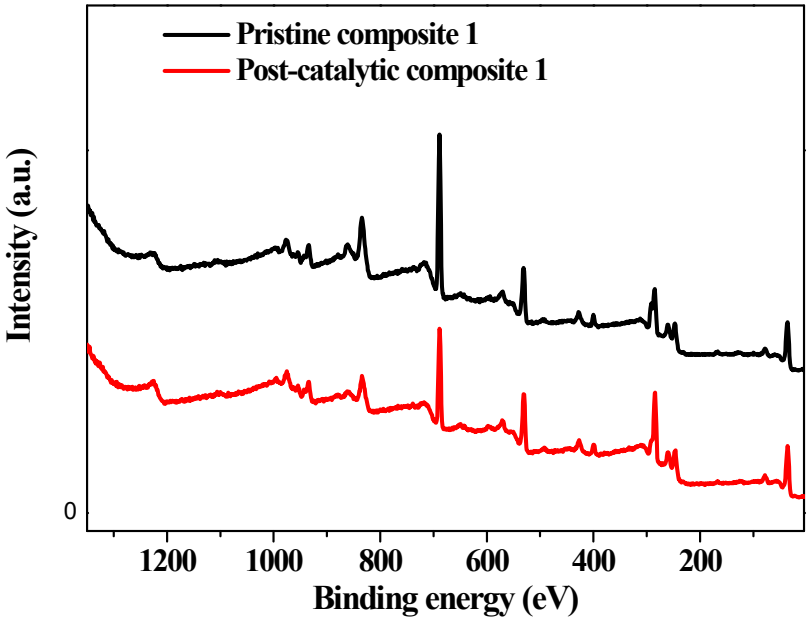

Fig. S20 XPS full scan spectra of pristine (top), post-catalytic composite **1** and polyoxometalate $K_8[SiW_{11}O_{39}]$ on FTO electrode used for CPE experiments at 1.40 V (vs. NHE) in PBS at pH of 6.5.

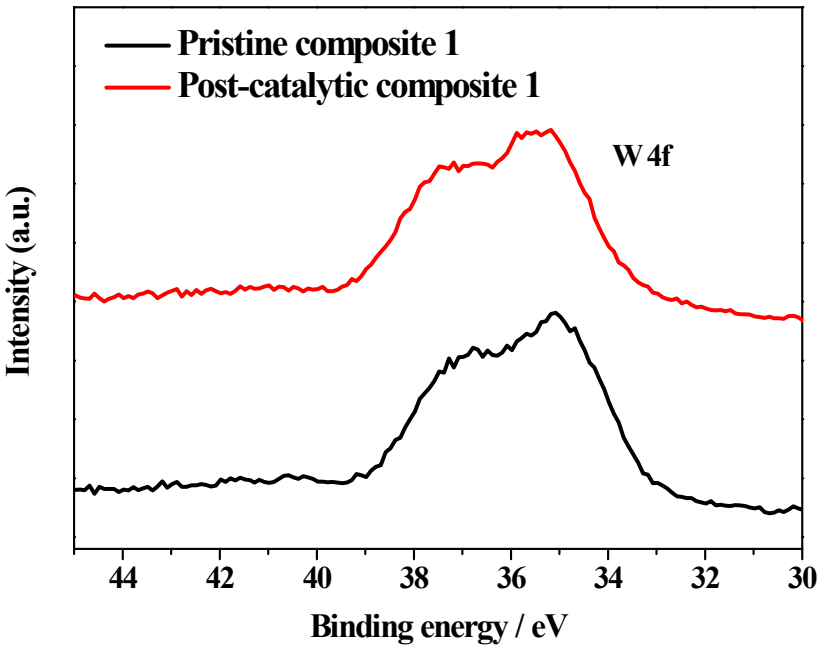

Fig. S21 High-resolution XPS W 4f spectra of pristine (bottom) and post-catalytic composite **1** on FTO electrode used for CPE experiments at 1.78 V (vs. RHE) in PBS at pH of 6.5.

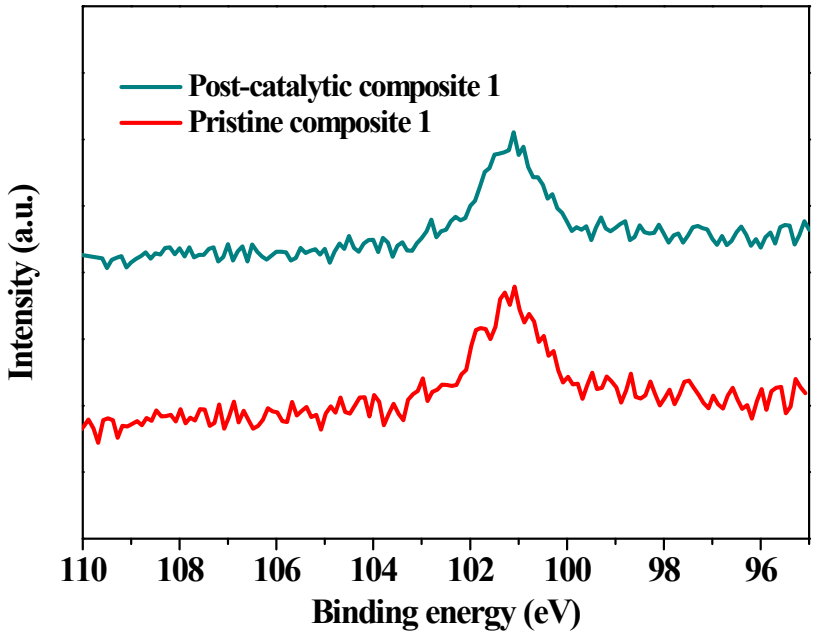

Fig. S22 High-resolution XPS Si 2p spectra of pristine (bottom) and post-catalytic composite **1** on FTO electrode used for CPE experiments at 1.78V (vs. RHE) in PBS at pH of 6.5.

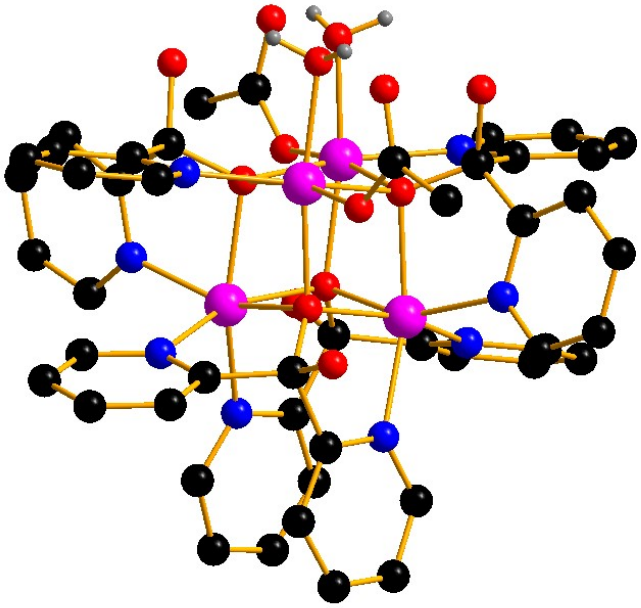

Fig. S23 The Ball-and-stick representation of $[Co_4(dpk{\cdot}OH)_4(OAc)_2(H_2O)_2]^{2+}$ studied in this work (pink, Co; black, C; red, O; blue, N, H atoms in ligand and counter cations ClO_4^- were omitted for clarity).

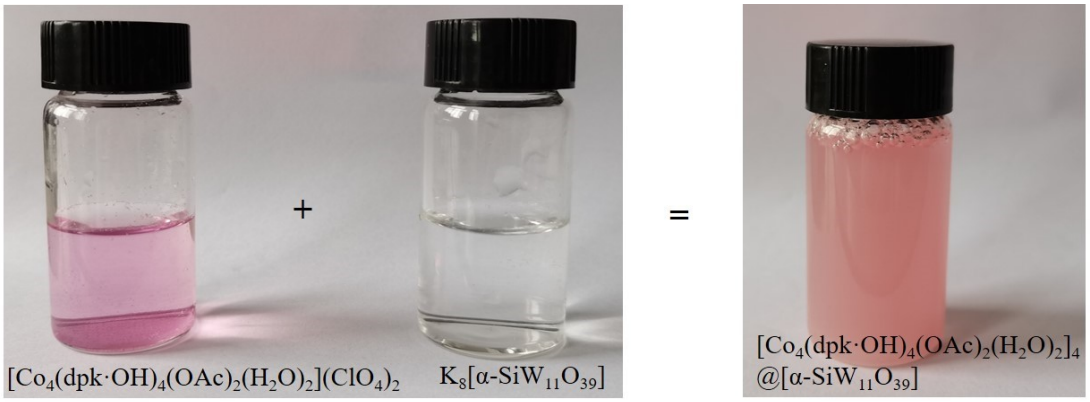

Fig. S24 Formation process of composite $[[Co_4(dpk{\cdot}OH)_4(OAc)_2(H_2O)_2]_4@[\alpha\text{-}SiW_{11}O_{39}]$ in water.

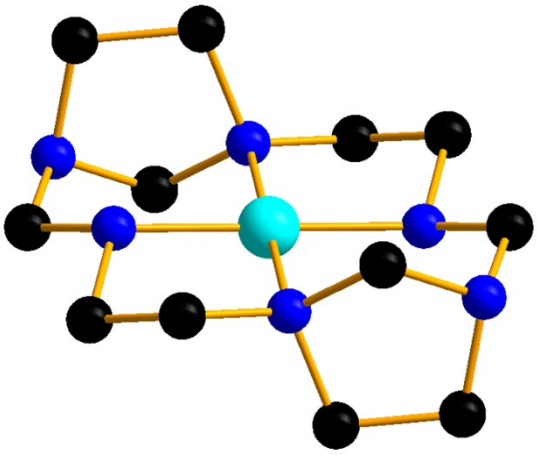

Fig. S25 The Ball-and-stick representation of $[Ni(NHA]^{2+}$ studied in this work (cyan, Ni; black, C; blue, N, H atoms in ligand and counter cations ClO_4^- were omitted for clarity).

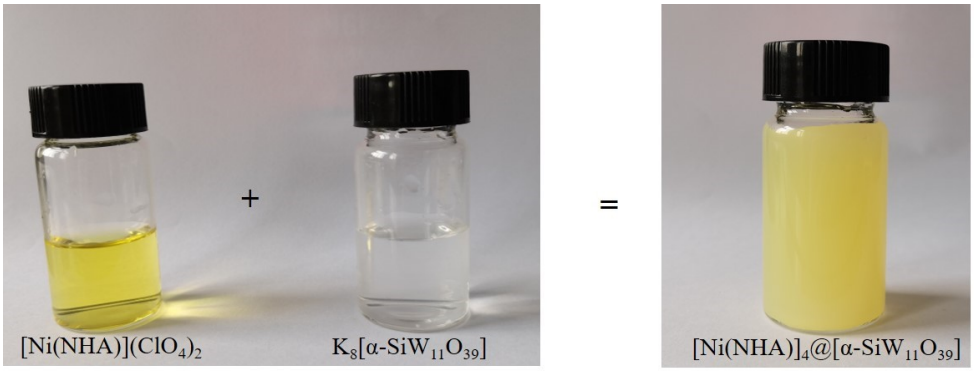

Fig. S26 Formation process of composite $[Ni(NHA)]_4@[\alpha\text{-}SiW_{11}O_{39}]$ in water.

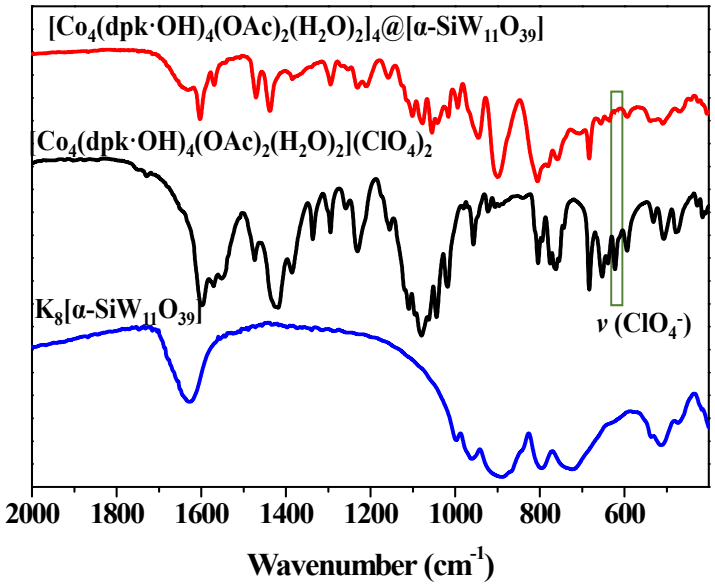

Fig. S27 FTIR spectra of composite $[Co_4(dpk{\cdot}OH)_4(OAc)_2(H_2O)_2]_4@[\alpha\text{-}SiW_{11}O_{39}]$ (red), $[Co_4(dpk{\cdot}OH)_4(OAc)_2(H_2O)_2](ClO_4)_2$ (black) and $K_8[\alpha\text{-}SiW_{11}O_{39}]$ (blue).

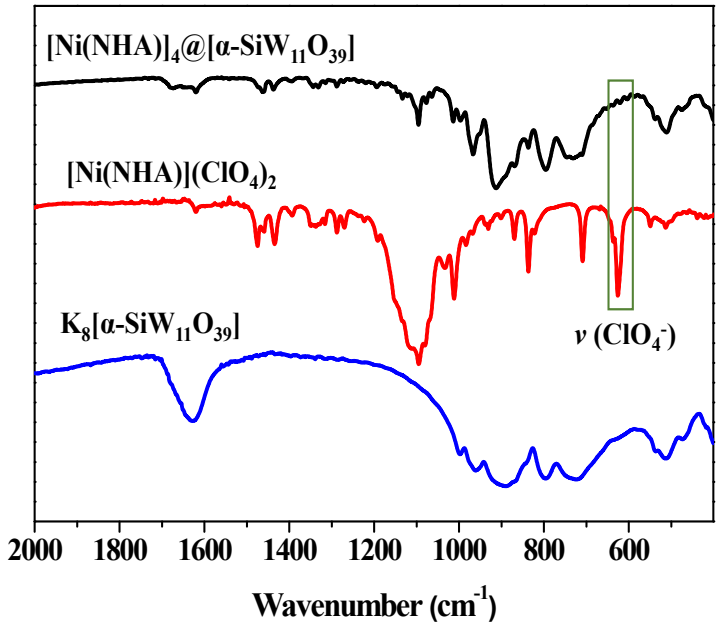

Fig. S28 FTIR spectra of composite $[Ni(NHA)]_4@[\alpha\text{-}SiW_{11}O_{39}]$ (black), $[Ni(NHA)](ClO_4)_2$ (red) and $K_8[\alpha\text{-}SiW_{11}O_{39}]$ (blue).

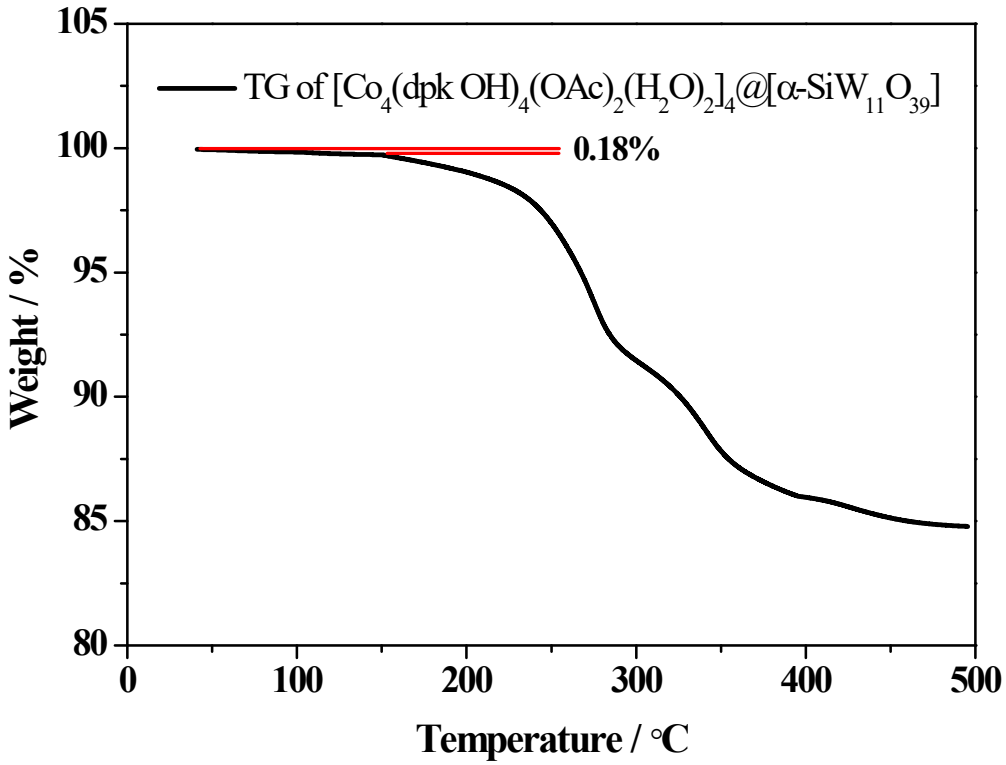

Fig. S29 TG analysis of Co-containing under N_2 atmosphere, temperature increasing rate: 10 °C / min.

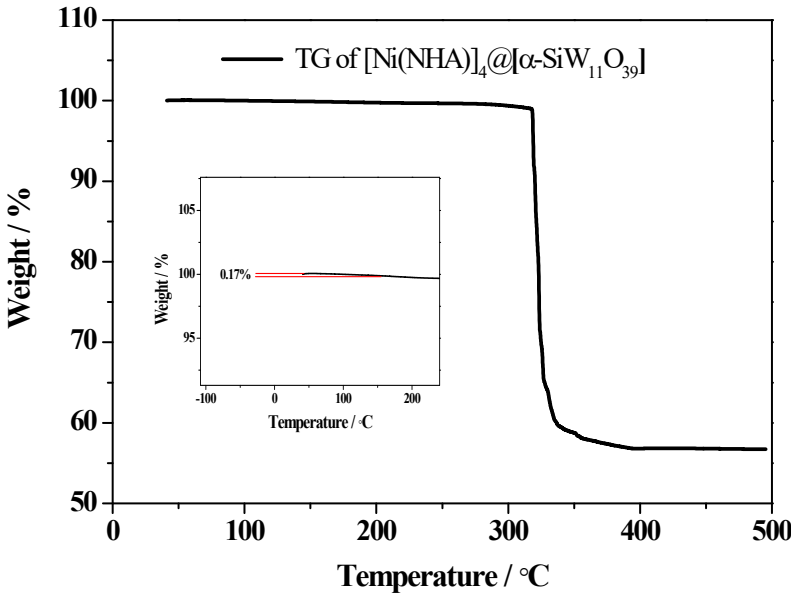

Fig. S30 TG analysis of Ni-containing under N_2 atmosphere, temperature increasing rate: 10 °C / min.

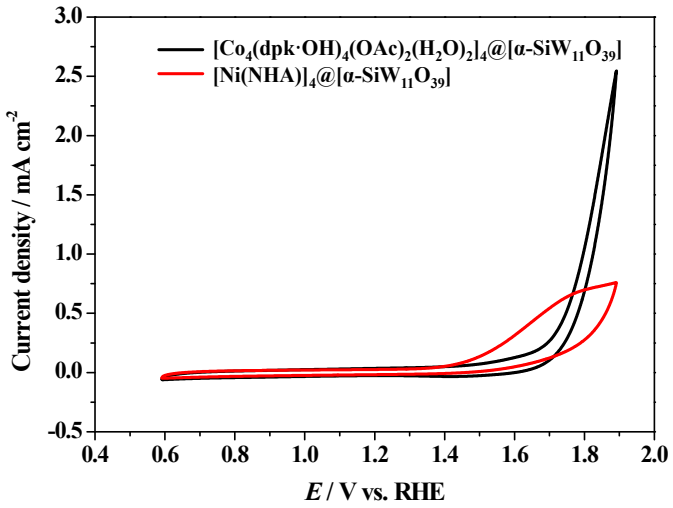

Fig. S31 Cyclic voltammograms of composite $[Co_4(dpk{\cdot}OH)_4(OAc)_2(H_2O)_2]_4@[\alpha\text{-}SiW_{11}O_{39}]$ and $[Ni(NHA)]_4@[\alpha\text{-}SiW_{11}O_{39}]$ in 0.1 M PBS at pH of 6.5, with GC electrode (0.071 cm^2) coated with composite as working electrode. scan rate=50 mV/s.

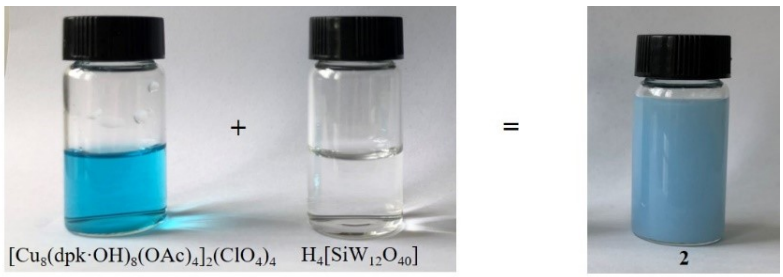

Fig. S32 Formation process of composite $[Cu_8(dpk{\cdot}OH)_8(OAc)_4]@[SiW_{12}O_{40}]$ in water.

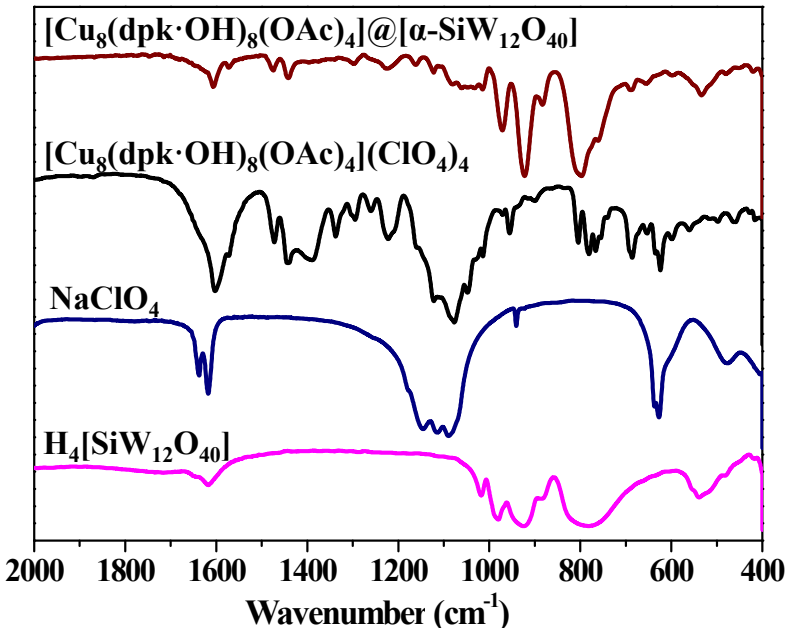

Fig. S33 FTIR spectra of composite $[Cu_8(dpk{\cdot}OH)_8(OAc)_4]@[SiW_{12}O_{40}]$ (brown), $[Cu_8(dpk{\cdot}OH)_8(OAc)_4](ClO_4)_4$ (black) and $H_4[SiW_{12}O_{40}]$ (pink).

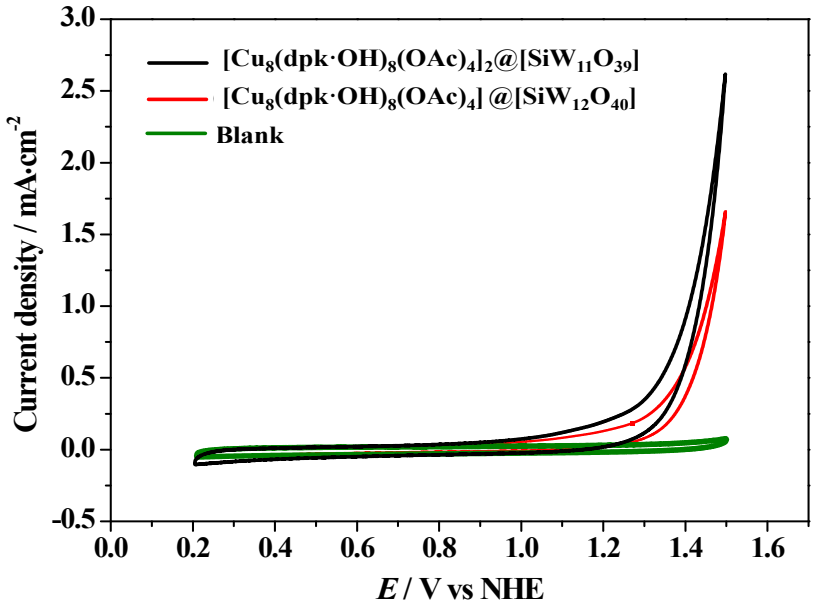

Fig. S34 Electrochemical test of composite $[Cu_8(dpk{\cdot}OH)_8(OAc)_4]_2@[\alpha\text{-}SiW_{11}O_{39}]$ and $[Cu_8(dpk{\cdot}OH)_8(OAC)_4]@[SiW_{12}O_{40}]$ in 0.1 M PBS at pH 6.5.

Table S1. Performance of some selected Cu-based heterogeneous catalysts in electrochemical water oxidation.

Catalyst	Electrolyte	pH	Current density (mA/cm^2)	η (mV)	Ref.
Cu-Bi film	0.2 M KBi	9.0	1.2	600	S1
CuO-based	0.1 M KBi	9.2	1.0	430	S2
CuO nanowires	0.1 M KBi	9.2	0.1	430	S3
Cu(TCA)-film	0.1 M Acetate buffer	6.0	1.0	720	S4
$Cu(OH)_2$	0.1 M KBi	9.2	0.1	550	S5
$[Cu_2\text{-}P_o]_n$	0.1 M KPi	9.2	1.0	644	S6
Cu_2O film	0.1 M KBi	9.2	1.0	450	S7
$Cu\text{-}CO_3$	0.5 M Na_2CO_3	10.8	1.0	485	S8
Cu-TEOA	0.1 M Acetate buffer	12.4	0.1	560	S9
$Cu(en)(OH_2)_4$	0.2 M PBS	12	1.0	540	S10
Cu-Gly film	0.2 M PBS	12	1.0	450	S11
Cu-Tris film	0.2 M PBS	12.4	1.0	390	S12
Composite **1**	0.1 M NaPi	6.5	1.0	580	This work

η = overpotential; HTCA = 1-mesityl-1H-1,2,3-triazole-4-carboxylic acid; en =1,2-ethylenediamine TEOA = triethanolamine; Gly = glycine; Tris = tris(hydroxymethyl)aminomethane.

References

S1 F. Yu, F. Li, B. Zhang, H. Li and L. Sun, *ACS Catal*., 2014, **5**, 627–630.

S2 X. Liu, S. Cui, Z. Sun, Y. Ren, X. Zhang and P. Du, *J. Phys. Chem. C*., 2016, **120**, 831–840.

S3 X. Liu, S. Cui, Z. Sun and P. Du, *Electrochim. Acta*., 2015, **160**, 202-208.

S4 H. A. Younus, Y. Zhang, M. Vandichel, N. Ahmad, K. Laasonen, F. Verpoort, C. Zhang and S. Zhang, *ChemSusChem*, 2020, **13**, 5088–5099.

S5 S. Cui, X. Liu, Z. Sun and P. Du, *ACS Sustainable Chem. Eng.*, 2016, *4*, 2593–2600.

S6 R. Mishra, E. Ülker and F. Karadas, *ChemElectroChem*, 2017, **4**, 75–80.

S7 X. Liu, Z. Sun, S. Cui and P. Du, *Electrochim. Acta*., 2016, **187**, 381-388.

S8 J. Du, Z. Chen, S. Ye, B. J. Wiley and T. J. Meyer, *Angew. Chem. Int. Ed*., 2015, **54**, 2073–2078.

S9 T.-T. Li, S. Cao, C. Yang, Y. Chen, X.-J. Lv and W.-F. Fu, *Inorg. Chem*., 2015, **54**, 3061–3067.

S10 C. Lu, J. Du, X.-J. Su, M.-T. Zhang, X. Xu, T. J. Meyer and Z. Chen, *ACS Catal*., 2016, **6**, 77–83.

S11 C. Lu, J. Wang and Z. Chen, *ChemCatChem*, 2016, **8**, 2165-2170.

S12 H. Chen, Y. Gao, Z. Lu, L. Ye and L. Sun, *Electrochim. Acta*., 2017, **230**, 501–507.